Atmos. Chem. Phys. Discuss., 11, 1641–1669, 2011
www.atmos-chem-phys-discuss.net/11/1641/2011/
doi:10.5194/acpd-11-1641-2011

Atmospheric Chemistry and Physics Discussions

Elevated aerosol layer embedded with aged soot particles in a polluted urban atmosphere

G. Shi[1], D. Zhang[2], B. Wang[1], B. Chen[1], M. Yamada[3], and H. Niu[4,2]

[1]LASG, Institute of Atmospheric Physics, Chinese Academy of Sciences, Beijing 100029, China
[2]Faculty of Environmental and Symbiotic Sciences, Prefectural University of Kumamoto, Kumamoto 862-8502, Japan
[3]Center for Innovation, Kanazawa University, Kanazawa 920-1192, Japan
[4]State Key Laboratory of Coal Resources and Safe Mining, College of Geoscience and Surveying Engineering, China University of Mining & Technology, Beijing 100083, China

Received: 16 December 2010 – Accepted: 4 January 2011 – Published: 19 January 2011

Correspondence to: D. Zhang (dzzhang@pu-kumamoto.ac.jp)

Published by Copernicus Publications on behalf of the European Geosciences Union.

Abstract

A layered structure of aerosol particles from surface to 1080 m was observed in Beijing during daytime on 8 December 2007. Under about 700 m, particles were well mixed vertically. From 700 to 1000 m was an elevated aerosol layer (EAL), in which aerosol concentration was remarkably larger than those in the lower and upper layers. Electron microscopic analysis of particles in the size range of 0.2~1.3 μm at different altitudes revealed that soot particles were predominant in all layers. There were fresh, young and aged soot particles in the lower layer. In contrast, soot particles in the EAL were all well aged, showing the structure of shrunk soot inclusions coated with weak absorbing species (the so-called core-shell structure). The geometric mean equivalent diameter of soot particles in the EAL was approximately 0.4~0.6 μm while that of their soot inclusions was about 0.1 μm. The EAL coincided with the remaining nocturnal layer aloft, which was the residual left by the daytime upward convective mixing in the boundary layer. The lapse rate in the lower part of the EAL had an obvious decrease in the morning, indicating the absorption effect of soot particles there. These results suggest that the fate of soot particles was closely dependent on the evolution of the boundary layer. While particles emitted from surface were efficiently mixed upward in daytime, residual nocturnal layer as a cap lid produced an EAL abundant in well-aged soot particles, in which the aerosols, as a feedback, enhanced the stability of the layer by absorbing solar radiation.

1 Introduction

Soot particles, emitted from biomass burning and fossil fuel combustion, have strong climate effects (Menon et al., 2002; Ramanathan and Carmichael, 2008) and constitute a substantial part of particulate matters to the air pollution in urban atmosphere (Molina and Molina, 2004; Chan and Yao, 2008). As a carrier of black carbon, soot is the strongest absorbing aerosol at the visible wavelength and its presence in the

ACPD
11, 1641–1669, 2011

atmosphere could significantly modify the transfer of solar radiation, the so-called aerosol direct effect on climate change (IPCC, 2007). Atmospheric aging processes convert the particles from hydrophobic to hydrophilic in a timescale of hours, which consequently increases the ability of absorbing incoming solar radiation, and enhances the ability of serving as nuclei for droplet formation to influence cloud properties, the so-called indirect effects (Moteki et al., 2007; Schwarz et al., 2008). On the other hand, emission of soot particles into urban atmosphere can reduce remarkably air quality (Song et al., 2006; Baumgardner et al., 2007), increase health risk, and cause public concern (Pope et al., 2009). Recent international field campaigns projecting to atmospheric aerosols always took soot particles and their subsequent effects as major subjects, such as the Smoke, Clouds, and Radiation – Brazil (SCAR – B) (Kaufman et al., 1998), the Aerosol Characterization Experiments – Asia (Huebert et al., 2003), and the Mexico City Metropolitan Area (MCMA) 2003 field campaign (Barnard et al., 2007). And understandings on soot properties and their atmospheric significance have been largely increased.

The effects of soot particles on climate and air quality depend not only on the physical and chemical properties of the particles but also on their temporal-spatial distributions (Gelencser, 2004). Dispersion and removal of the aerosol particles in the air are governed closely by flow and disturbance (Seinfeld and Pandis, 1998). As primary particles, soot particles are originally emitted into the air from ground sources, except a small fraction from aviation. Their vertically upward dispersion in the boundary layer via turbulence and thermal eddies is the first step for them to travel within local, regional and large scales. The evolution of the thermodynamic structure of the boundary layer regulates the movement of particles there, and consequently, the temporal-spatial distributions of soot particles are closely relevant to the structure of the boundary layer (Siebert et al., 2004).

In general, the evolution of the thermal dynamic structure of atmospheric boundary layer under clear conditions is dependent on the diurnal variation of the solar heating to the surface. It is the ground that warms and cools in response to the radiation, which in

ACPD
11, 1641–1669, 2011

turn forces changes in the boundary layer via transport processes (Stull, 1988). After sunrise in the morning, the surface is warmed due to the absorption of solar energy. Upward mixing from surface is triggered although the mixing layer is still shallow for calm situations at this stage. As the air is warmed through turbulent mixing, the convection near the surface becomes vigorous and the mixing layer extends to hundreds of meters or even 1∼2 km for wind situations. The strong turbulence homogenizes pollutants in the convective mixing layer. Just before sunset, the generation of the thermals in the mixing boundary layer is shut off due to the cooling of surface and the turbulence cannot be maintained against dissipation. In the absence of the mechanical forcing, temperature fluctuations decay fast, turbulence in the mixed layer soon decays completely, and the surface layer becomes stably stratified as a residual layer. Nighttime cooling of the surface due to the lack of energy supply and the loss of energy via thermal infrared radiation stabilizes the near-surface air further and changes the whole boundary layer into a nocturnal inversion, in which only stratified flow may appear in a few cases (Stull, 1988).

In response, the vertical distribution of pollutants in the boundary layer must have been consistent with the boundary variation (Liu et al., 2009). For example, trapping of pollutants into the lower stable layer by an inversion lid at the top of boundary layer is common in high-pressure regions. If the convective mixing developing from surface after sunrise penetrates the stable layer and breaks the inversion lid with strong vertical mixing or overshooting, pollutants emitted from surface will be distributed widely. Otherwise, the pollutants will be confined under the inversion layer, which sometimes leads to pollution alerts in local areas.

On the other hand, model simulations with speculated conditions showed that absorbing aerosols within the atmospheric boundary layer decrease the probability of formation of boundary layer clouds, causing additional warming through cloud-feedbacks (Yu et al., 2002). The result is very sensible to the vertical distribution of aerosols. Absorbing aerosols above the boundary layer can lead to the increase of the strength of capping inversion and the reduction of radiative flux at the surface. Aerosols in the

ACPD
11, 1641–1669, 2011

boundary layer absorb the solar radiation, stratifying the air and inducing feedbacks on the surface energy partitioning. All of these weaken the surface buoyancy flux, consequently lowering the top of the boundary layer and compressing pollutants within the layer.

Therefore, investigation of the dependence of the properties and distributions of soot particles on the evolution of the thermodynamic structure of atmospheric boundary layer can greatly contribute to understanding the climate and environmental effects of anthropogenic particles and restraining uncertainties in relevant studies. Unfortunately, very few field data on this subject are available. This is because most observations of aerosol particles in elevated layers were carried out with aircraft-borne instruments, which could not show the structure of the boundary layers near the surface. Although remote sensing with satellite data or lidar signals can provide the vertical profiles of aerosol particles in the atmosphere, the accuracy of the profiles closely depends on the schema used in the retrieval which needs to be verified with field data.

Several observations on the vertical distribution and the structure of the boundary layer were carried out in Beijing, the capital city of China, with tethered balloon flights. In the flights on 8 December 2007 when it was clear and a middle latitude anticyclone dominated the synoptic scale weather, an elevated aerosol layer was encountered near the top of the mixing layer and particle samples were successfully collected below, in and above the layer. The subsequent dedicated analyses revealed the details of the properties of particulate matters at different levels and the evolution of the thermodynamic structure of the boundary layer. In this paper, we report the results and discuss the responses of the particles' properties to the boundary layer structure.

2 Method

A tethered balloon system was applied to measure aerosol particles and meteorological conditions as the balloon ascended and descended in the range from ground to up to~1200 m altitude at a speed about 1~4 m s^{-1}. The observation was held at Beijing

ACPD
11, 1641–1669, 2011

Meteorological Observatory (39°48′ N; 116°28′ E; 33 m a.s.l.; WMO Station Number: 54511) in Beijing, the capital city of China, on 8 December 2007, when Beijing and the surrounding areas were covered by an anticyclone system with its center to the north of Beijing and the center pressure about 1040 hPa. The weather was fine and the wind speed near the ground was very weak. The balloon system was ascended and descended with the reference to the real time wind profiles. At the site, wind profiles were monitored with a wind profiling system (CFL-16, China Aerospace Science & Industry Corp.), which provided the horizontal and vertical wind from 150 m to about 6000 m with a vertical resolution of 150 m every 6 min.

On-board instruments included a portable optical particle counter, two low volume aerosol samplers, and a meteorological radiosonde. The radiosonde (GTS1; Tianxi Electric Instrument Factory) was provided by the meteorological observatory and it measured temperature, pressure, humidity at a time resolution of 1 s. Signals from it were recorded by a receiving system on the ground and the altitude of the tethered balloon system from ground was automatically calculated by the receiving system with the static equilibrium equation.

The particle counter (HHPC-6 Utility, ART Instruments Inc., USA) measured the size-segregated particle number concentration of aerosol particles continuously with a time resolution of 1 min without delay. The measurement diameter ranges of the particle counter are 0.3–0.5, 0.5–0.7, 0.7–1.0, 1.0–2.0, 2.0–5.0, and >5.0 µm.

Aerosol particles were collected onto electron microscope meshes which were coated with carbon-sprayed Formvar film by using the samplers. Each low volume sampler was equipped with a two-stage impactor. The jet diameters of the first and second stages of the impactor are 1.3 and 0.4 mm, respectively, and the flow rate was 2.2 l min^{-1}. Assuming a unit particle density, the aerodynamic diameters at which particles can be collected with 50% efficiency are approximately 1.3 and 0.2 µm under standard atmospheric conditions. That means particles of diameter larger than 1.3 µm would have been efficiently collected onto meshes set at the first stage and particles of 0.2~1.3 µm onto the meshes at the second stage. Although particles smaller than

ACPD
11, 1641–1669, 2011

0.2 µm could be trapped by the second stage meshes, the smaller the particles, the larger their loss. Details of the setup of the balloon system were similar to that described by Matsuki et al. (2005).

Three flights were held from the morning to the afternoon. Table 1 shows the flight information. In each flight, the balloon system was ascended gradually to the maximum altitude and stopped there. Then one particle sampler was switched on by a remote controller and started to collect a set of samples of the first and second stages for 3 min. After that, the balloon system was gradually descended to another altitude, where the other sampler collected a set of samples again. After the particle collection, the balloon system gradually descended to the ground and the meshes in the impactors were replaced. Then, another flight was started. In total, six sets of samples were obtained at different altitudes (Table 1) during the three flights.

Particles on the meshes were photographed and analyzed using a transmission electron microscope (TEM; JOEL: JEM-1210), and a scanning electron microscope (SEM; PHILIPS, XL-30) which is coupled with an energy dispersive X-ray spectrometer (EDX; Phoenix). The EDX spectrometer can detect elements with atom numbers larger than 5 in a single particle on the meshes.

Particles were characterized by their electron images and elemental composition. Photos of particles were randomly taken from each sample while trying to cover particles as much as possible. To obtain the statistical characteristics in size, shape, and category of the particles, every particle in each photo was carefully investigated by measuring the on-film shape and size. The particles were first categorized according to their morphologies. Then for each category, tens of the particles were analyzed by using the EDX spectrometer to confirm whether particles in the same category had similar elemental composition.

ACPD
11, 1641–1669, 2011

3 Results

3.1 Elevated aerosol layer (EAL)

The maximum altitudes of the flights were 880 m, 1080 m and 280 m. Here and also in the following descriptions, the unit is barometric meter. Figure 1 shows the vertical profiles of the number concentrations of particles in different size ranges, temperature, and relative humidity at the ascent of flight 2. An elevated aerosol layer (EAL) was encountered between 700 m and 1000 m, below and above which the concentration of aerosol particles was apparently smaller than in the EAL. Aerosol concentrations in each size range at different altitudes from surface to about 700 m were approximately similar and, above 1000 m, the concentrations of particles dramatically decreased with altitudes, indicating particles were well vertically mixed under 700 m and the layer above 1000 m was isolated from the EAL. Temperature in the EAL was approximately the same without apparent decrease or increase with altitude, suggesting it was a very strong stable layer. At 150 m, there was a thin inversion layer, which was expected to be the result of wind shear near the surface. Therefore, below 700 m was the convective mixing layer and above 1000 m was the low free troposphere.

The particle number-size distributions at the altitudes of particle collection are illustrated in Fig. 2. In the diameter range of 0.5~2.0 µm, the particle concentrations in the EAL at 740 m and 890 m were much higher than those at other altitudes. Around 0.3 µm and 3.0 µm, the concentrations at different altitudes were approximately the same except those at 1080 m. Actually, the concentration of particles in the size range of 0.3~2.0 µm in the EAL was 350~450 cm^{-3}, while the concentration in the lower layers was 220~260 cm^{-3} and, to the extent of the available data, 60~70 cm^{-3} in the upper layers. In the diameter range of >5.0 µm, the concentrations varied and were small, except that the concentration at 740 m was a little high.

Accumulation of secondary particles in smaller size ranges were unlikely responsible for the high concentration in the diameter range of 0.5~2.0 µm in the EAL. This is because particles with the size of 0.3~0.5 µm had similar concentration at

ACPD
11, 1641–1669, 2011

different altitudes in the whole boundary layer. If the particles in the diameter range of 0.3~0.5 µm in the EAL had accumulated to produce particles in the range of 0.5~2.0 µm there, the concentrations in this size range at 50 m, 280 m and 550 m should have had similar values to those in the EAL. In this regard, the high concentration of aerosols in the EAL must be caused by other atmospheric processes.

3.2 Characteristics of particles in the EAL

The six sets of aerosol samples were obtained at 880 m, 740 m, 1080 m, 550 m, 280 m, and 40 m, respectively (Table 1 and Fig. 1). In the collection order, samples of set 1 and set 2 were collected at 880 m and 740 m in the EAL, and samples of set 3 at 1080 m in the lower free troposphere. Samples of set 4, set 5, and set 6 were collected at 550 m, 280 m, and 40 m, respectively, in the lower layer near the surface where particles were well vertically mixed. Since a very small number of particles were observed on the first stage meshes and they were not statistically meaningful, here we concentrate on the particles collected on the second stage meshes. Note that, according to the estimation, particles in the aerodynamic diameter range of 0.2~1.3 µm were efficiently trapped on the meshes.

Figure 3 shows the examples of transmission electron microscope pictures of particles at 550 m, 740 m, 880 m and 1080 m. Pictures of particles at 280 m and 40 m are not shown because the morphology of particles at the two altitudes was similar to that of particles at 550 m. The particles in the EAL show an image of a core circled with an outside ring, i.e. the particles had a core-shell structure, suggesting they were aged ones (particles marked by arrows in Fig. 3b and c). The cores were electron opaque and looked like aggregates or shrunk chains of multiple spherules, and the outside circles were composed of weak-electron-absorption components. In contrast, the image of particles in the lower layer was more complex and had shapes of aggregates, patches of fragments or small spots (marked in Fig. 3d). In the upper layer, almost all particles were in a round shape but did not have obvious cores or inclusions (marked in Fig. 3a).

ACPD
11, 1641–1669, 2011

The EDX analysis revealed that the major elements in the core parts of core-shell particles and the particles in chain-like or aggregate shapes were oxygen and carbon, indicating they were originally soot particles. This is not surprising because similar particles have been frequently observed in polluted urban atmosphere (e.g., Johnson et al., 2005). The core-shell structure indicates that the particles had been well changed due to aging in the atmosphere, while chain-like and aggregate particles were in the stages of young and fresh (Posfai et al., 2004; Kocbach et al., 2005). Condensation of sulfate, nitrate, ammonium, and volatile organic compounds on soot particles has been proved to be responsible for the aging of the particles (Ammann et al., 1998; Zhang et al., 2001; Shi et al., 2008; Khalizov et al., 2009; Kiselev, 2010; Pratt and Prather, 2010).

Besides the soot particles described above, there were a large number of particles which were small spots and electron-weak-absorption particles, such as the marked particles in Fig. 3d. Their size was in the range of submicron meters or smaller. No elements were detectable in such particles except oxygen in a few particles. These particles are believed to be produced via the growth or accumulation of secondary particles, which could be found in any urban atmosphere. In addition, flying ash and road dust were also found in the samples.

The number fractions of different kind particles were roughly estimated from particles' image of the transmission electron microscope pictures. Soot particles were always the majority and predominant in the size range of 0.2~1.3 μm in all layers. They occupied approximately 92% at 280 m (220 particles), 88% at 550 m (168 particles), 79% at 740 m (197 particles), 75% at 880 m (248 particles), and 90% at 1080 m (313 particles). Thus most of the accumulation mode particles between 0.2 and 1.3 μm were actually soot particles. In particular, in the EAL, the soot particles were round shaped by aging with condensation and coagulation and they were responsible for the high concentrations of aerosols there, which is consistent with the previous expectation from the size distribution.

ACPD
11, 1641–1669, 2011

3.3 Size distributions from TEM analysis

The effective diameter range of particle collection by the second stage is 0.2~1.3 µm. This is estimated from the pump rate, nozzle diameter, and particle density with the assumption that all particles are spherical in the air. Electron microscopic pictures show particles on the collecting film and the collected particles were frequently in round or nearly-round shape (Fig. 3). The images on the film were residues of evaporation and most of the particles must have been in aqueous phase before being captured. Assuming that such particles on the film after impaction were hemi-spherical with their volume equal to that before being captured, the on-film diameter of a particle should be approximately 1.3 of their geometric diameters in the air. Particles in aqueous phase must expand more or less after being captured on the film. Consequently, the on-film diameter of a particle should not be smaller than 1.3 of its geometric diameter in the air, i.e. the estimation from the on-film diameter shows the upper bound of the geometric size of a particle. Here we size the particles with their on-film diameters divided by 1.3 and the size is described as equivalent diameter. The on-film diameter of the particle is the diameter of a circle which has the same area as the projection area of the particle on the film.

With the ratios of the equivalent diameters of core parts to the equivalent diameters of the particles, the aged statuses of soot particles at different altitudes were investigated. Figure 4 shows the number frequencies according to the ratio at different altitudes. Note that the maximum of the ratio is 1, and the smaller the ratio is, the smaller the core is in comparison to the whole particle. Here we consider that the aged status of the particles is inversely proportional to the ratio. In addition, the distribution at 1080 m is not available because the images of particles there frequently showed in a state of opacity and did not have a clear core-shell structure (refer to Fig. 3a). At 280 m, the ratios were mainly in the range of 0.4~0.9 with the maximum between 0.7 and 0.8, indicating that the core size of most soot particles at this altitude was approximately the same as or larger than the half of the same particles. At 550 m, more

ACPD
11, 1641–1669, 2011

particles were in the range of 0.1∼0.3, that means the aged status was a little more severe in comparison with particles at 280 m. The distributions in the EAL were very different from the lower layer. No particles were in the range of 0.9–1, indicating that all particles had clear core-shell structure. Maximum ratios at both 740 m and 880 m were in the range of ∼0.1, indicating that the core size of many particles was less than one-tenth of their size, i.e. the particles at these altitudes had been largely amplified by secondary species and water vapor. Therefore, soot particles in the EAL had been modified by aging processes much more severe than those in the lower layer.

The core-shell structure of the aged soot particles was further investigated with the tentative number-size distributions of the particles and their core parts. Lognormal functions (Baron and Willeke, 2001) (the distributions were presumably lognormal) were applied to fit the distributions. Figure 5 shows the distributions, their fitting curves, and the geometric mean diameters of the fitting distributions. Particle numbers were normalized to 100 in the calculation and the distributions are tentative ones. The geometric mean diameters of the aged soot particles in the EAL were remarkably larger than those of aged soot particles in the lower layer. In contrast to that the diameters at 550 m and 280 m were about 0.3 µm where the distributions were very similar, the diameters at 740 m and 880 m in the EAL were 0.4∼0.6 µm. However, the geometric mean diameters of the core parts at 880 m, 740 m and 550 m were similar, about 0.1 µm, and that at 280 m was a little larger (about 0.2 µm). The difference between the geometric mean diameter of the particles and that of the core parts was 0.31 µm at 880 m, 0.48 µm at 740 m, 0.16 µm at 550 m, and 0.13 µm at 280 m.

These results indicate that the variation of soot particles due to aging in the EAL was the largest compared to that in the lower layer. Aging had caused the original soot particles to shrink into aggregates and their size shifted to smaller range. At the same time, condensation and coagulation of secondary species and water vapor caused a substantial growth of the particles in size. In summary, aging transformed the particles into aqueous phase with the shrunk soot cores as inclusions and resulted in the size of the inclusion cores much smaller than the whole particles. These results

ACPD
11, 1641–1669, 2011

also indicate that aged soot particles are very effective medium for secondary species formation or water vapor condensation even in very dry air (the relative humidity was less than 30% in the EAL: Fig. 1). In addition, the modification of soot particles in the lower layer was not as severe as in the EAL but aging had also been processed obviously.

4 Discussion

4.1 Formation of the EAL

The evolution of the thermodynamic structure of the boundary layer from the morning was investigated with the meteorological data of the first and second flight. Results show that the EAL coincided with the residual layer of the nocturnal stable layer which had not been eroded completely by the upward convection starting from the surface. Figure 6 shows the vertical profiles of virtual potential temperature and mixing ratio of water vapor of the first and second flights. For reference, the profiles of the number concentration of particles in the size range of 0.3~1.0 µm are also shown in the figure. The vertical profiles of flight 3 (its maximum altitude was 280 m) were similar to that of the lower part of the descending of flight 2.

At the time of the first flight ascending, the layer from surface to about 210 m was approximately adiabatic with a constant mixing ratio, indicating that solar heating of the surface had triggered the start of convective mixing and resulted in the development of statically unstable mixing layer close to the ground. From 210 m up to the maximum altitude (~880 m), the virtual potential temperature (θ_v) indicates a stable structure of the layer. However, the stable layer was separated into three sub layers by two thin sharp shifts: one at 395~410 m and another at 650~660 m. From 210 m to 395 m, the stability was very weak with a θ_v increase of less than 0.2 K (approximately 0.1 K/100 m) and it was approximately adiabatic. In contrast, the layer from 410 m to 650 m was fairly stable with a θ_v increase of about 2.6 K (1.1 K/100 m). Above 660 m up to 880 m,

ACPD
11, 1641–1669, 2011

the layer was also very stable although the decrease of θ_v (0.9 K/100 m) was a little weaker than the adjacent below layer. The mixing ratio (q) kept almost constant and aerosol concentrations at different altitudes were approximately similar from the surface to 650 m, which also indicate a strong vertical mixing in this layer. Above 660 m, both q and aerosol concentration showed clearly different distributions from those in the lower layer, indicating the vertical mixing had not reach above 660 m. Therefore, the layer from surface to 410 m should be the convective surface mixing layer (marked by ML in the figure) and the layer from 410 m to 660 m was an entrainment zone (EZ). Above 660 m should be the remaining part of the nocturnal stable layer, which was being eroded by the upward convection (RL). Similar structure was also confirmed at the descending of the first flight, except that the ML became a little thicker, the EZ ascended approximately 10 m and the boundary between the ML and the EZ was clearer than that at the flight ascending.

The whole structure of the boundary layer was obtained by the second flight. At the ascending of the flight, the ML had extended to 580 m but its development due to vertical mixing likely ceased because the EZ from 580 m to 720 m was vague and the downward mixing from the high level (or the overshooting from the low level) was weak. This was further evidenced by the structure at the flight descending. At the time of the descending, the EZ had vanished and the ML and EZ had combined to become a new residual layer (marked by nRL). At the same time, a thin stable layer between the ground and the RL appeared. Above 720 m, the RL existed and its thickness was approximately 330 m (720–1050 m), which coincided with the EAL. This was similar to the one encountered in the first flight. Above the RL, it was the lower free troposphere (FT) where the aerosol concentration decreased abruptly compared to those in the lower layers.

These results indicate that the EAL was the upper part of the nocturnal stable layer. Even when the development of upward mixing ceased in the afternoon, overshooting of lower level mixing had not consumed the nocturnal layer completely. Consequently, a residual nocturnal stable layer was left aloft during the daytime, in which no mixing in

ACPD
11, 1641–1669, 2011

vertical directions was expected. Thus the soot particles in the EAL, i.e. the particles at 740 m and 880 m, must be input there by the upward mixing on the previous day and were kept aloft by the layer since then. In contrast, the particles in the layer below 740 m, i.e. the particles at 550 m and 280 m, contained both the particles in the nocturnal layer and the particles upward lifted by the mixing on the observation day. This means that the residence time of all primary particles in the EAL was about one day or longer while that of a large fraction of particles at lower levels was hours. This is consistent with the difference of the aged statuses between the aerosols in the EAL and the mixing layer. Soot particles in the EAL were completely aged ones while particles in the mixing layer included fresh, young and aged ones.

4.2 Aging and subsequent effects

As discussed in previous sections, sulfur and nitrogen chemistry in association with ammonium is suggested to be mainly responsible for the aging of the soot particles. This is further supported by the fact that, in addition to carbonaceous species, sulfate, nitrate and ammonium always contribute substantially to the particulate matters in Beijing (Hu and Guo, 2009). The EDX analysis in this study confirmed the frequent presence of sulfur in the observed soot particles at each level. In addition, solar radiation could result in photochemical reactions among the constituents in the residual layer during day time to enhance the formation of secondary aerosols. This is considered to be the reason that there were also a large number of secondary particles in the EAL besides soot particles, although we did not discuss them in details. High concentration of secondary particles would favor the growth of aged soot particles via adsorption of the new particles.

The soot particles in the EAL and the lower mixing layer had very different size-segregated distributions. However, the distributions of core parts at the middle of mixing layer (550 m) was similar to that in the EAL but different from that at the lower level of the mixing layer (280 m) (Fig. 5). The residence time of soot particles at 550 m was in a scale of hours. This was much shorter than that of particles in the EAL, which

ACPD
11, 1641–1669, 2011

was in a scale of day. Considering the fact that the soot particles in the lower mixing layer would stay aloft even after the mixing layer became nocturnal stable, they would be further aged in the way of the particles in the EAL, i.e. the soot particles at 550 m would probably repeat the fate of the soot particles in the EAL. Thus differences of the distributions suggest that further aging of the particles at 550 m would cause the increase of their shell parts but could not result in considerable changes of the core parts. As a result, the core-shell structure is likely a very good but simple model for well-aged soot particles in the boundary layer. In the size range of 0.2~1.3 µm, soot parts in aged particles keep a lognormal distribution with the geometric mean diameter around 0.1 µm. Any changes corresponding to particle size, such as evaporation and condensation of volatile species, would only cause the change of the shell parts of the particles. In this regard, an aged soot particle could be considered as a core of primary mass with coating of secondary species and water vapor in the investigation of its activities in cloud droplet formation as a nucleus.

Although the particles in the EAL were mainly in the submicron range and had spherical shape, they were not secondary particles but primary particles coated heavily with secondary species and liquid water. An important implication of this result is that appearance of submicron spherical particles in elevated layers or near surface in polluted urban atmosphere, which were frequently observed with other approaches such as lidars and particle counters near the surface, could not be simply attributed to the formation of new particles in accumulation mode. The evolution of thermal dynamic structure of the boundary layer must be considered in order to identify the origin of the particles. In the present case, lidar observation close to the site at Beijing on the day revealed the presence of a layer of spherical particles at the altitudes of the EAL (unpublished data, available from N. Sugimoto, NIES of Japan).

It is likely there was a feedback between the aerosol and the thermal structure of the EAL. In general, the static stability of typical residual nocturnal layers during daytime is neutral and the dry adiabatic lapse rate is approximately 0.98 K/100 m. However, the average lapse rate of temperature of the lower part of the EAL, where the concentration

ACPD
11, 1641–1669, 2011

of aerosols increased rapidly with altitude, was 0.53 K/100 m (linear regression between 650 m and 780 m) at the first flight ascending, −0.81 K/100 m (between 670 m and 880 m) at the first flight descending, −0.45 K/100 m (between 740 m and 880 m) at the second flight ascending, and −0.88 K/100 m (between 710 m and 840 m) at the second flight descending. These lapse rates were all much smaller than the dry adiabatic lapse rate, and even smaller than 0.65 K/100 m, the lapse rate of standard atmosphere in the clear troposphere at the radiative equilibrium. The decrease of the rate in the morning indicates an upper level warming or a lower level cooling in the layer. Since it was in the daytime under clear conditions, cooling in elevated layers in lower troposphere was not expected. There was no latent heat released into the EAL because of the cloud-free conditions. Sensible heat from the upper layer was not anticipated. The only available explanation is that the layer was heated by downward and upward radiation and the strong inversion was the absorption effect of the radiation. Soot particles are strong absorbing aerosols because of their black carbon content. It has been suggested that aging of soot particles and the core-shell structure will further enhance their absorption ability (e.g., Moffet and Prather, 2009). The appearance of soot particles in elevated layers under cloud-free conditions can result in heating effects. For these reasons, the strong static stability of the EAL was considered to be the result of the absorption effects of the aged soot particles there. The stable layer, acting like a blanket, could reduce more or less solar radiation to the surface and suppress the development of the lower mixing layer, which would, in turn, weaken the upward mixing and tend to stabilize the boundary layer. This feedback effect has been suggested in recent model works by Yu et al. (2002) and Pandithurai et al. (2008), and the results here are observational evidences.

In addition, the results indicate that the aging of soot particles reduced the size of soot parts in the particles and the shrinkage of the soot parts was accomplished rapidly. The soot parts kept approximately stable after the shrinkage while the shell parts continued to increase due to the production of secondary species or the absorption of water vapor leading to the growth of the particles in size. Deliquescence of soot

ACPD
11, 1641–1669, 2011

particles increases the particles' ability of absorption while the coating increases the ability of scattering. Therefore, the size ratio of soot parts to shell parts representing the aged statuses of the particles could be a key factor in the investigation of the activities of soot particles in the atmospheric mass cycles and radiative forcing.

5 Conclusions

Aerosol particles at different altitudes from the surface to 1080 m were measured with tethered balloon-borne instruments at Beijing on 8 December 2007 when the synoptic scale weather was dominated by an anticyclone and it was clear. As the balloon ascended and descended, particle number concentrations and the thermodynamic structure of the boundary layer were measured. Aerosol samples were collected at different altitudes and were later analyzed by using electron microscopes. An EAL was encountered between 700~1000 m, in which aerosol concentrations were much larger than the lower and upper layers. Aged soot particles in core-shell structures were the majority in the size range of 0.2~1.3 μm and, out of this size range, few soot particles were detected. It was confirmed from the evolution of the thermodynamic structure of the boundary layer that the EAL coincided with the residual layer of nocturnal boundary layer left by the upward mixing from surface in the daytime and the aged soot particles enhanced the inversion in the layer by absorbing solar radiation. Aging of the soot particles in the EAL shaped the particles into spherical shape in submicron size range, suggesting that increase of accumulation mode particles in elevated layers in polluted urban atmosphere was not always due to new particle formation. Comparisons of the aged statuses of the soot particles at different altitudes revealed that soot parts in the particles shrank rapidly to a steady size while the shell parts could continue to increase due to the condensation of volatile species leading to the growth of the particles in size.

ACPD
11, 1641–1669, 2011

Acknowledgements. The authors would like to thank Jay Melton for his review of word and grammar. This study was supported by China's 973 Plan under No. 2006CB403706, Grant-in-Aid for Scientific Research (C) of JSPS under No. 21510021, and MOST Project 2009DFA22650.

References

Ammann, M., Kalberer, M., Jost, D. T., Tobler, L., Rossler, E., Piguet, D., Gaggeler, H. W., and Baltensperger, U.: Heterogeneous production of nitrous acid on soot in polluted air masses, Nature, 395, 157–160, doi:10.1038/25965, 1998.

Barnard, J. C., Kassianov, E. I., Ackerman, T. P., Johnson, K., Zuberi, B., Molina, L. T., and Molina, M. J.: Estimation of a "radiatively correct" black carbon specific absorption during the Mexico City Metropolitan Area (MCMA) 2003 field campaign, Atmos. Chem. Phys., 7, 1645–1655, doi:10.5194/acp-7-1645-2007, 2007.

Baron, P. A. and Willeke, K.: Aerosol Measurement, 2nd edn., John Wiley, Hoboken, NJ, 2001.

Baumgardner, D., Kok, G. L., and Raga, G. B.: On the diurnal variability of particle properties related to light absorbing carbon in Mexico City, Atmos. Chem. Phys., 7, 2517–2526, doi:10.5194/acp-7-2517-2007, 2007.

Chan, C. K. and Yao, X.: Air pollution in mega cities in China, Atmos. Environ., 42, 1–42, doi:10.1016/j.atmosenv.2007.09.003, 2008.

Gelencser, A.: Carbonaceous Aerosol, Springer, Dordrecht, The Netherlands, 2004.

Hu, M. and Guo, S.: Particle pollution in Beijing: features, source and secondary formation, Newsl. Int. Global Atmos. Chem. Proj., 42, 10–18, 2009.

Huebert, B. J., Bates, T., Russell, P. B., Shi, G., Kim, Y. J., Kawamura, K., Carmichael, G., and Nakajima, T.: An overview of ACE-Asia: strategies for quantifying the relationships between Asian aerosols and their climatic impacts, J. Geophys. Res., 108, 8633, doi:10.1029/2003JD003550, 2003.

IPCC: Climate Change 2007: The Physical Science Basis, Contribution of Working Group I to the Fourth Assessment Report of the Intergovernmental Panel on Climate Change, edited by: Solomon, S., Qin, D., Manning, M., Chen, Z., Marquis, M., Averyt, K. B., Tignor, M., and Miller, H. L., Cambridge University Press, Cambridge, UK and New York, NY, USA, 2007.

Johnson, K. S., Zuberi, B., Molina, L. T., Molina, M. J., Iedema, M. J., Cowin, J. P., Gaspar, D. J.,

ACPD

11, 1641–1669, 2011

Wang, C., and Laskin, A.: Processing of soot in an urban environment: case study from the Mexico City Metropolitan Area, Atmos. Chem. Phys., 5, 3033–3043, doi:10.5194/acp-5-3033-2005, 2005.

Kaufman, Y., Hobbs, P. V., Kirchhoff, V. W. J. H., Artaxo, P., Remer, L. A., Holben, B. N., King, M.D., Ward, D. E., Prins, E. M., Longo, K. M., Mattos, L. F., Nobre, C. A., Spinhirne, J. D., Ji, Q., Thompson, A.M., Gleason, J. F., Christopher, S. A., and Tsay, S.-C.: Smoke, Clouds, and Radiation – Brazil (SCAR – B) experiment, J. Geophys. Res., 103, 31783–31808, doi:10.1029/98JD02281, 1998.

Khalizov, A. F., Zhang, R., Zhang, D., Xue, H., Pagels, J., and McMurry, P. H.: Formation of highly hygroscopic soot aerosols upon internal mixing with sulfuric acid vapor, J. Geophys. Res., 114, D05208, doi:10.1029/2008JD010595, 2009.

Kiselev, A., Wennrich, C., Stratmann, F., Wex, H., Henning, S., Mentel, T. F., Kiendler-Scharr, A., Schneider, J., Walter, S., and Lieberwirth, I.: Morphological characterization of soot aerosol particles during LACIS Experiment in November (LExNo), J. Geophys. Res., 115, D11204, doi:10.1029/2009JD012635, 2010.

Kocbach, A., Johansen, B. V., Schwarze, P. E., and Namork, E.: Analytical electron microscopy of combustion particles: a comparison o vehicle exhaust and residential wood smoke, Sci. Total Environ., 346, 231–243, 2005.

Liu, P., Zhao, C., Zhang, Q., Deng, Z., Huang, M., Ma, X., and Tie, X.: Aircraft study of aerosol vertical distributions over Beijing and their optical properties, Tellus B, 61, 756–767, doi:10.1111/j.1600-0889.2009.00440.x, 2009.

Matsuki, A., Iwasaka, Y., Shi, G.-Y., Chen, H.-B., Osada, K., Zhang, D., Kido, M., Inomata, Y., Kim, Y.-S., Trochkine, D., Nishita, C., Yamada, M., Nagatani, T., Nagatani, M., and Nakata, H.: Heterogeneous sulfate formation on the dust surface and it dependency on the mineralogy: observational insight from the balloon-borne measurements in the surface atmosphere of Beijing, China, Water Air Soil Pollut., 5, 101–132, 2005.

Menon, S., Hansen, J., Nazarenko, L., and Luo, Y.: Climate effects of black carbon aerosols in China and India, Science, 297, 2250–2253, doi:10.1126/science.1075159, 2002.

Moffet, R. C. and Prather, K. A.: In-situ measurements of the mixing state and optical properties of soot with implications for radiative forcing estimates, P. Natl. Acad. Sci. USA, 106, 11872–11877, doi:10.1073/pnas.0900040106, 2009.

Molina, M. J. and Molina, L. T.: Megacities and atmospheric pollution, J. Air Waste Manage., 54, 644–680, 2004.

ACPD
11, 1641–1669, 2011

Moteki, N., Kondo, Y., Miyazaki, Y., Takegawa, N., Komazaki, Y., Kurata, G., Shirai, T., Blake, D. R., Miyakawa, T., and Koike, M.: Evolution of mixing state of black carbon particles: Aircraft measurements over the Western Pacific in March 2004, Geophys. Res. Lett., 34, L11803, doi:10.1029/2006GL028943, 2007.

Pandithurai, G., Seethala, C., Murthy, B. S., and Devara, P. C. S.: Investigation of atmospheric boundary layer characteristics for different aerosol absorptions: case studies using CAPS model, Atmos. Environ., 42, 4755–4768, 2008.

Pope, C. A., Ezzati, M., and Dockery, D. W.: Fine-particulate air pollution and life expectancy in the United States, New Engl. J. Med., 360, 376–386, 2009.

Posfai, M., Gelencser, A., Simonics, R., Arato, K., Li, J., Hobbs, P. V., and Buseck, P. R.: Atmospheric tar balls: particles from biomass and biofuel burning, J. Geophys. Res., 109, D06213, doi:10.1029/2003JD004169, 2004.

Pratt, K. A. and Prather, K. A.: Aircraft measurements of vertical profiles of aerosol mixing states, J. Geophys. Res., 115, D11305, doi:10.1029/2009JD013150, 2010.

Ramanathan, V. and Carmichael, G.: Global and regional climate changes due to black carbon, Nat. Geosci., 1, 221–227, doi:10.1038/ngeo156, 2008.

Seinfeld, J. H. and Pandis, S. N.: Atmospheric Chemistry and Physics: From Air Pollution to Climate Change, John Wiley, Hoboken, NJ, 1998.

Schwarz, J. P., Spackman, J. R., Fahey, D. W., Gao, R. S., Lohmann, U., Stier, P., Watts, L. A., Thomson, D. S., Lack, D. A., Pfister, L., Mahoney, M. J., Baumgardner, D., Wilson, J. C., and Reeves, J. M.: Coatings and their enhancement of black carbon light absorption in the tropical atmosphere, J. Geophys. Res., 113, D03203, doi:10.1029/2007JD009042, 2008.

Shi, Z., Zhang, D., Ji, H., Hasegawa, S., and Hayashi, M.: Modification of soot by volatile species in an urban atmosphere, Sci. Total Environ., 389, 195–201, 2008.

Siebert, H., Stratmann, F., and Wehner, B.: First observations of increased ultrafine particle number concentrations near the inversion of a continental planetary boundary layer and its relation to ground-based measurements, Geophys. Res. Lett., 31, L09102, doi:10.1029/2003GL019086, 2004.

Song, Y., Zhang, Y. H., Xie, S. D., Zeng, L. M., Zheng, M., Salmon, L. G., Shao, M., and Slanina, S.: Source apportionment of $PM_{2.5}$ in Beijing by positive matrix factorization, Atmos. Environ., 40, 1526–1537, 2006.

Stull, R. B.: An Introduction to Boundary layer Meteorology, Kluwer Academic Pub., Dordrecht, The Netherlands, 1988.

ACPD
11, 1641–1669, 2011

Yu, H., Liu, S. C., and Dickinson, R. E.: Radiative effects of aerosols on the evolution of the atmospheric boundary layer, J. Geophys. Res., 107, 4142, doi:10.1029/2001JD000754, 2002.
Zhang, D., Iwasaka, Y., and Shi, G.: Soot particles and their impacts on the mass cycle in the Tibetan atmosphere, Atmos. Environ., 35, 5883–5894, 2001.

ACPD
11, 1641–1669, 2011

Table 1. Flight time (Beijing standard time: GMT + 08:00), sampling altitudes (in barometric meters), and the surface weather conditions during each flight. The samples are numbered by circled numbers according to the order of collection.

	Flight time		Sampling altitude		Surface weather condition				
	Ascending	Descending	(m)		T(°C)	RH(%)	P(hPa)	WS(m s^{-1})	WD
Flight 1	11:16–12:10	12:14–13:20	①880	②740	2.7–4.4	30–25	1025.3–1023.4	1.5–2.1	SW–SW
Flight 2	14:02–14:49	14:53–15:58	③1080	④550	5.3–5.3	24–25	1022.8–1022.0	1.4–0.7	SW–NW
Flight 3	16:16–16:24	16:29–16:44	⑤280	⑥40	5.3–4.9	25–26	1022.0–1022.1	0.8–1.4	NE–N

ACPD
11, 1641–1669, 2011

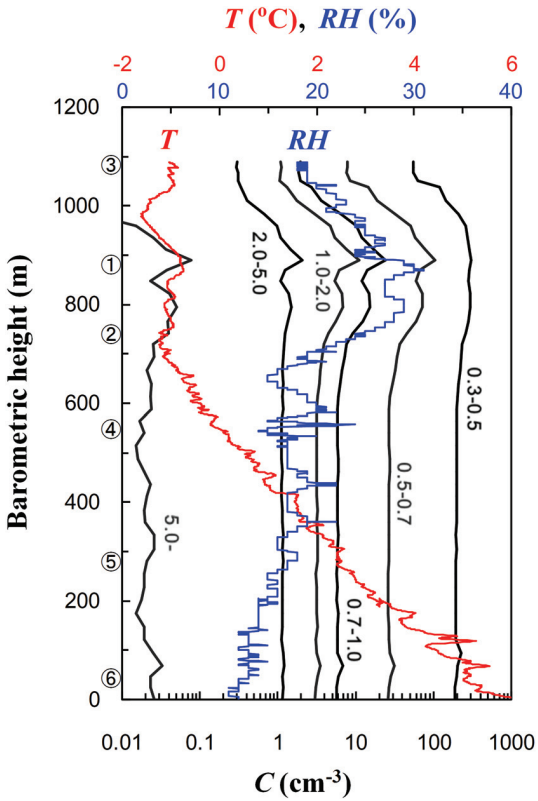

Fig. 1. Vertical profiles of temperature (T), relative humidity (RH) and size-segregated particle number concentrations (C) at the ascending of flight 2. Altitudes of the particle collection are marked by circled numbers in the order of collection (Table 1).

ACPD
11, 1641–1669, 2011

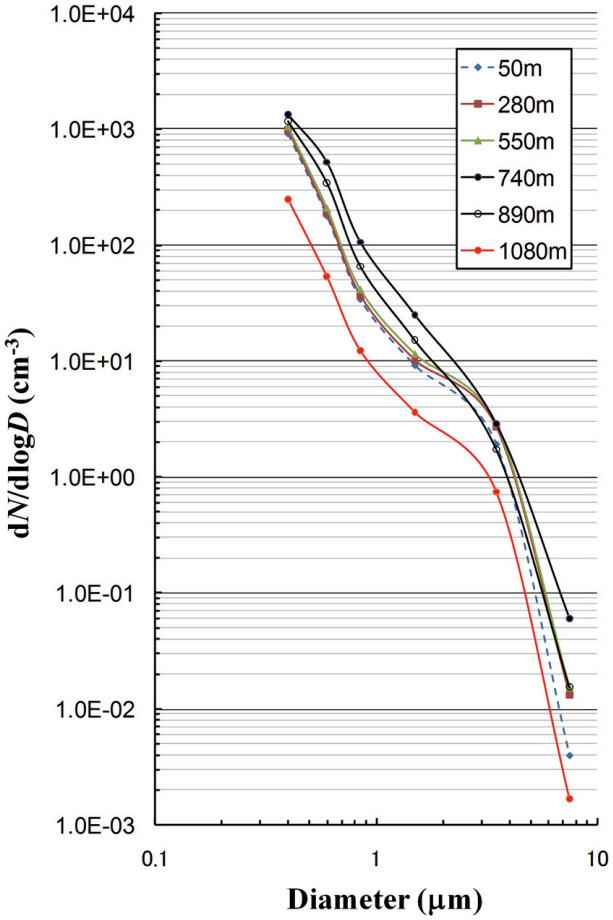

Fig. 2. Number-size distributions of particles from the optical particle counter at different altitudes of particle collection. The concentrations used for the distribution calculation are the average during the 3 min particle collection for each sample.

ACPD
11, 1641–1669, 2011

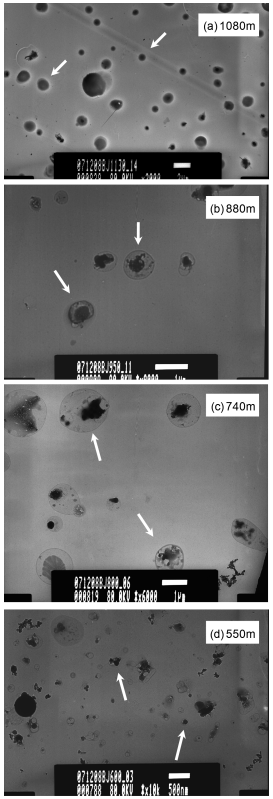

Fig. 3. Examples of the electron microscope pictures of particles in the samples at 550 m, 740 m, 880 m and 1080 m. Scale bar is 2 μm in **(a)**, 1 μm in **(b)**, 1 μm in **(c)**, and 0.5 μm in **(d)**.

ACPD
11, 1641–1669, 2011

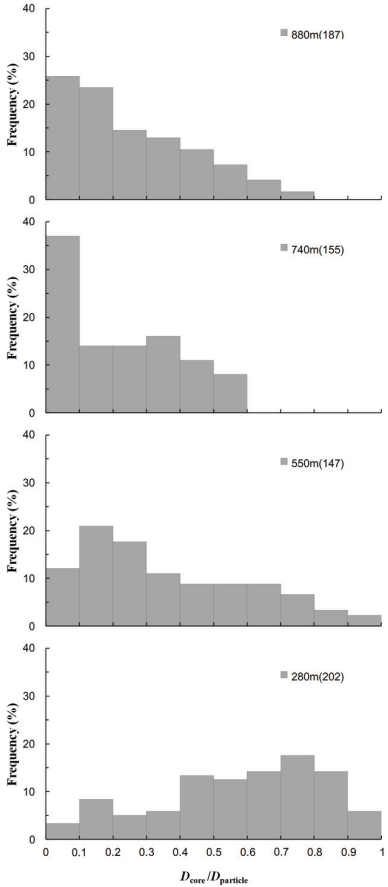

Fig. 4. Frequencies of soot particles at each altitude in the equivalent diameter range of 0.2~1.3 μm according to the ratios of their core size (D_{core}) to particle size ($D_{particle}$). The size of a particle was determined from its image in the electron microscope picture (see the text for details). The numbers of particles are shown in the parentheses.

ACPD
11, 1641–1669, 2011

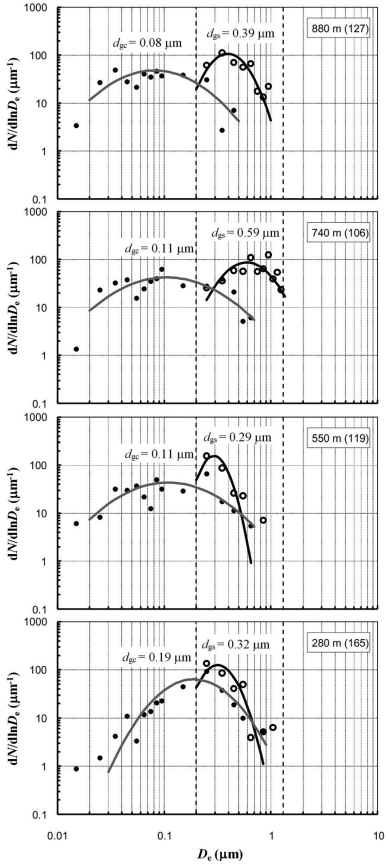

Fig. 5. Tentative number-size distributions of core-shell soot particles (circles) and the core parts of the same particles (dots), and their fitting curves. The numbers of particles are listed in the parentheses and were normalized to 100 in the distribution calculation. The geometric mean diameter (d_{gs} for soot particles and d_{gc} for core parts) of each fitting curve is shown above the curve.

ACPD
11, 1641–1669, 2011

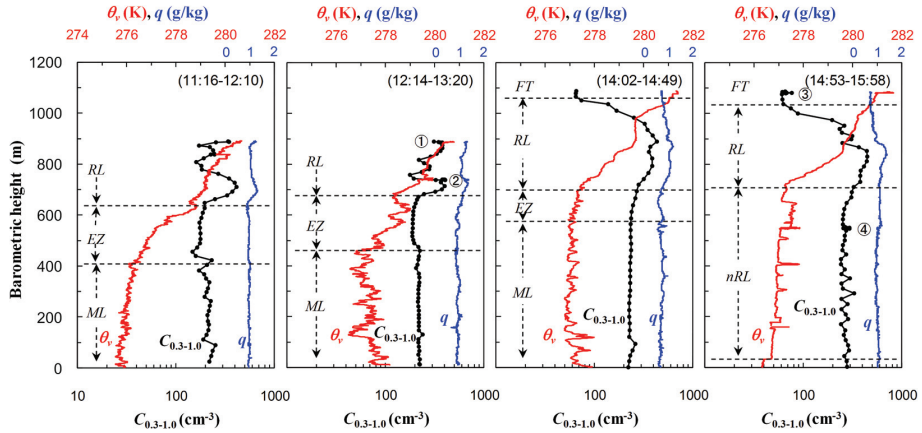

Fig. 6. Vertical profiles of the virtual potential temperature (θ_v), water vapor mixing ratio (q), and the aerosol number concentrations in the size range of 0.3~1.0 µm ($C_{0.3\sim1.0}$) in the first and second flights (Table 1). Ascending and descending time of each flight is shown in the figure.

ACPD
11, 1641–1669, 2011